An Experimental Investigation of Brittle Failure Mechanisms in Scratch Tests of Rock

He Zhang[a], Jia-Liang Le[a], Emmanuel Detournay[a,*]

[a]*Department of Civil, Environmental, and Geo- Engineering, University of Minnesota, Minneapolis, MN 55455, USA*

Abstract

This paper reports the results of scratch tests on three rocks (Bonne Terre Dolomite, Alabama Marble and Dunnville Sandstone) conducted at depths of cut ranging from 0.2 mm to 2.6 mm. The experiments were performed on slabs of thickness slightly smaller than the cutter width, with a camera recording the entire cutting process. The test results reveal the existence of three cutting regimes: ductile, fragmentation, and brittle with increasing depth of cut. The regimes differ by the failure mode, the dependence of the specific energy ϵ on the depth of cut d, and the fragment shapes. In the ductile regime, $\epsilon \sim d^0$ and the fragments are constitutive grains of the rock or powder as a result of intense shearing. In the fragmentation regime, $\epsilon \sim d^{-1/2}$ and the fragments is a mix of ductile-type particles and flake-like chips also the product of shear failure. Finally, the brittle regime is characterized by $\epsilon \sim d^{-1}$ and is essentially associated with chip-like fragments that come in two varieties depending on whether they are created by shear or by tension. The d^{-1}-dependence of the specific energy can only be observed if the rock is sufficiently homogeneous at the scale of the experiment. The distinction between different modes of failure is based on evidence from video recording and fractography with a Scanning Electron Microscope. It is shown that the dominance of tensile over shear fracture is intimately related to the existence of a crushed zone, which acts as a wedge to initiate a tensile macrocrack in a compressive stress field. Finally, an analysis of the energy partitioning in the brittle regime indicates that the energy dissipated in creating new surfaces with a tensile crack is actually negligible compared to the energy expended in the formation of the wedge. This result indicates that the mode I toughness cannot be determined from the specific energy in the brittle regime, on the basis of a model of a crack parallel

*Corresponding author
Email address: detou001@umn.edu (Emmanuel Detournay)

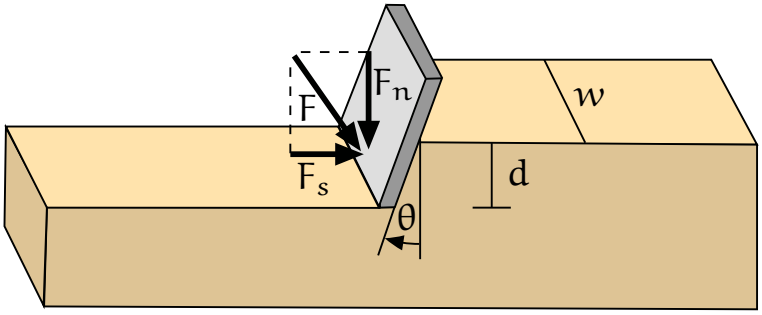

Figure 1: Sketch of the cutter-rock interaction.

to the free surface, in contradiction with published claims to that effect. Finally, this experimental investigation clarifies some confusion in the literature, rooted on assuming the existence of only two modes of failure, ductile and brittle.

Keywords: Scratch test, Rock cutting process, Failure mode, Fracture toughness, Specific energy, Fragmentation

---

1. Introduction

The scratch test involves shaving rock from the surface of a sample by moving a cutter in a direction parallel to the free surface. The test is conducted under kinematic control, with the depth of cut d and the cutter velocity V imposed and maintained constant along the entire cut. The tangential (or cutting) force F_s and normal force F_n acting on the moving cutter are continuously measured during the test (see Fig. 1). Typically, the depth of cut imposed in scratch testing varies between about 0.1 mm to a few mm. As an experimental technique, the scratch test has been widely used to study the rock cutting process, primarily to gain insights into the rock breaking mechanisms with the goal of improving the efficiency of mechanical excavation by optimizing the cutting tools and the operational parameters [1–5].

The geometry of the rectangular cutters commonly used in a scratch test is simply described by width w and back-rake angle $\theta > 0$, with the cutter inclined forward with respect to the direction of motion as illustrated in Fig. 1. Scratch tests can be divided into two types, depending on whether the cutter width is larger or smaller than the thickness of the rock specimen. For the first type, slabs of thickness slightly smaller than w are used for the experiments so that there is no sidewall effects. Hence the cutting force are expected to be proportional to w in view of the apparent two-dimensional nature of the process. For the second type, the cutter is tracing a groove at the surface of the rock specimen; the presence of sidewalls then introduce

a dependence of the cutting force on the ratio d/w, presumably caused by the additional frictional resistance due to the transverse normal stress generated by bulking of the fragmented rock [6].

An important indicator of rock cuttability is the specific energy ϵ, defined as the energy required to cut a unit volume of rock. Previous investigations have shown that the scaling of the specific energy with respect to the depth of cut is closely related to the failure modes [7, 8]. At shallow depth of cut (typically larger than the rock grain size and less than 1 mm for a medium strength rock), the rock is intensively sheared ahead of the cutter in a continuous manner so that no particular events can be isolated while cutting. This cutting mode, defined as ductile, is characterized by continuous de-cohesion of the constitutive matrix and grains, with grains and powders accumulating progressively in front of the cutter. Consensus on the independence of specific energy ϵ upon the depth of cut d in the ductile regime has been reached on the basis of an extensive laboratory experimental program involving the testing of several hundred rocks [9]. The constant specific energy ϵ in the ductile regime is found to be well correlated with the rock uniaxial compressive strength (UCS).

As the depth of cut d increases beyond a critical depth of cut d_*, the failure process is associated with the continuous formation of thin flake-like fragments [8, 10] together with debris similar to those generated in the ductile regime. The particle size distribution follows a power law over a significant range of sizes [11]. The increasing size of the largest fragments with d leads to a decrease of the specific energy with respect to the depth of cut. Interestingly, laboratory scratch tests on several types of rock have provided substantial evidence that the scaling of the specific energy ϵ with respect to depth of cut d follows $\epsilon \sim d^{-1/2}$ in this regime, as shown in Fig. 2 in magenta color. Scratch tests on several types of rock reveal a consistent rock failure pattern in the fragmentation regime, i.e., the formation of thin flake-like fragments, a consequence of the branching, interaction and propagation of a system of microcracks caused by the compression imparted by the cutter motion.

As the depth of cut increases above a second critical depth of cut d_{**}, the fragmentation regime eventually disappears and is replaced by the brittle regime. This regime is characterized by the discontinuous formation of large rock chips with the simultaneous presence of small fragments and debris and by a steeper decrease of the specific energy with the depth of cut compared to the fragmentation regime. As shown in Fig. 2, the scaling law for the specific energy follows $\epsilon \sim d^{-1}$ in the brittle regime for scratch tests on homogeneous rocks. Unlike the scaling law of the specific energy in the fragmentation regime, which generally follows $\epsilon \sim d^{-1/2}$ for several different types of rock, the $\epsilon \sim d^{-1}$ relationship may not hold for heterogeneous rocks in

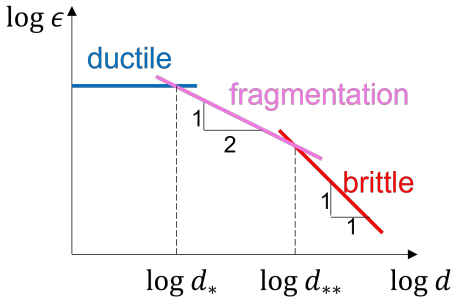

Figure 2: Scaling law of specific energy ϵ with respect to depth of cut d in three failure regimes. The specific energy ϵ is constant in the ductile regime, and follows $\epsilon \sim d^{-1/2}$ and $\epsilon \sim d^{-1}$ in the fragmentation and brittle regimes, respectively.

the brittle failure regime due to the co-existence of different failure patterns, leading to a random and inconsistent rock cutting process over the rock sample lengths used in small scale tests.

Previous studies have considered only two distinct modes of failure, ductile and brittle [7, 8, 12–17]. However, different interpretations of the brittle regime have led to some confusion. The distinction between a ductile regime characterized by a specific energy independent of the depth of cut and a brittle regime (now referred to as the fragmentation regime) for which the specific energy decreases as the inverse of square root of depth of cut was originally proposed by Detournay and co-workers based on laboratory experiments with rectangular cutters [7, 8, 11, 12, 14]. They noted consistency between experimental evidence and arguments invoking scaling and minimum energy principle. Indeed a linear dependence of the cutting force on d for a cutter of width w implies that the prefactor to the group dw has dimension FL^{-2} like the compressive strength q, while a linear dependence of F_s on $\sqrt{d}$ implies that the prefactor of the group $d^{1/2}w$ has dimension $FL^{-3/2}$ like the toughness K_c. Finally, they noted that the transition depth of cut d_* between these two force models naturally scales by K_c^2/q, with the cutting force corresponding to ductile failure being smaller than the cutting force for the brittle failure if d is less than d_*, and vice versa if d is larger than d_*.

Confusion about the brittle regime was set off by incorrectly attributing to the $\epsilon \sim d^{-1/2}$ regime the formation of tensile cracks sub-parallel to the free surface that were observed in cutting experiments [8, 11, 13, 18, 19]. This confusion fueled claims that toughness could be determined from the cutting force measured in scratch experiments in the $\epsilon \sim d^{-1/2}$ regime, based on a mathematical model constructed on the premise that the cutting energy is entirely dissipated in the propagation of subhorizontal tensile macrocracks [13, 20, 21]. These claims have generated robust

debates and discussions in the literature [22–28]. In fact, as indicated above and demonstrated experimentally in this paper, the propagation of a macro-tensile crack sub-parallel to the free-surface is observed in the $\epsilon \sim d^{-1}$ regime (provided that the rock is homogeneous at the scale of the experiments) and not in the $\epsilon \sim d^{-1/2}$ fragmentation regime.

A critical aspect of rock cutting in the brittle regime, which is not addressed in the above references, is the mechanism of initiation of a sub-horizontal tensile crack in a compressive stress field. According to several studies [10, 14, 29–31], the initiation of a tensile crack is actually closely related to the formation of a crushed zone ahead of the cutting tool. This zone acts as a wedge to induce a tensile crack. It is observed that the rock in the crushed zone is pulverized into fine powders due to the compressive stress concentration so that intensive energy is dissipated in the formation of the crushed zone [29, 32–34]. Visual evidence of the formation of the crushed zone obtained with high-speed camera [35, 36] or a workshop microscope [29] have been reported. Moreover, according to [35, 37], the size of the crushed zone determines whether tensile fracture or shear/compression failure dominates the mechanism of rock failure in the brittle regime. Factors that affect the size of the crushed zone include the pressure at the cutter/rock contact surface, the relationship between the depth of cut and the cutter width, the cutter geometry, the friction between the crushed rock and the cutter face, and the rock properties [29, 33].

In summary, interpretation of the scratch test suffers from ambiguity in the classification of rock failure modes and a lack of consensus about the underlying rock failure mechanisms in the fragmentation and brittle modes. This state of affair has led to a misinterpretation of the scratch tests results and misleading conclusions regarding which rock mechanical properties can be assessed from these tests. To address these issues, a comprehensive campaign of scratch tests was carried out on slabs of different rock types to explore the transition between different rock failure modes with an emphasis on the fragmentation and brittle regimes. A camera was used to record the entire cutting process in order to visualize the failure macro-mechanisms. Rock cuttings from the fragmentation and brittle regimes were collected and fracture surfaces of two distinct chip morphologies were examined with a Scanning Electron Microscope (SEM). In addition, the measured cutting force signals were synchronized with the recorded videos so as to provide detailed information regarding the force response in relation to rock chipping and thus useful insights into the brittle failure of rocks in the cutting process. The partition of cutting energy in scratch tests conducted in the brittle regime was assessed to examine the validity of the assumption that the cutting energy is mostly dissipated in creating new crack surfaces as the tensile crack propagates.

The paper is organized as follows. Section 2 introduces the experimental apparatus, preparation of the slab rock samples, and the test procedure. The classification of three different rock failure regimes are described in Section 3 according to the observation from the recorded video and the scaling law of specific energy versus depth of cut. The assesment of rock heterogeneity is discussed in Section 4 by low-pass filtering of the force signals obtained in the ductile regime. Section 5 presents results of scratch tests in the fragmentation regime with a discussion on the force signals and rock failure mechanism. The brittle failure mode is elaborated in detail in Section 6 with focus on different rock chipping patterns controlled by different failure mechanisms. Section 7 outlines an analysis for the cutting energy partition. Finally, conclusions are drawn in Section 8.

2. Rock Cutting Tests

2.1. Experimental Apparatus

The tests were conducted with the Wombat, a rock scratcher manufactured by EpsLog, see Fig. 3a. The main components of the scratcher are [9]: a test bed used to secure a slab holder, a moving cart supporting a load cell, a cutter, and a vertical positioning system. The horizontal movement of the cart is set at an imposed constant speed by means of a computer controlled stepper motor driving a ball screw via a gearbox. The depth of cut is adjusted manually by means of a crank mechanism fixed to an Archimedes screw, and a micrometer displays the value of depth of cut. A locking system is utilized to prevent the cutter vertical movement in order to maintain a constant depth of cut while cutting.

A custom-designed metal holder was manufactured to firmly secure the rock slab using several one-sided socket bolts (see Fig. 3b). The motion and rotation of rock slab are thus prevented during testing. To avoid potential damage of the rock samples, two metal shims were used in between the rock slab and the holder such that the concentrated bolt forces applied by a torque wrench were converted into a more uniform pressure. The shim thickness was selected to ensure that the cutter width covers the entire thickness of the slab to avoid any sidewall effects. The metal holder was then firmly attached to the test bed of the Wombat with several socket bolts.

Scratch tests were carried out using a sharp rectangular cutter with a width of 10 mm and a rake angle of 15°(see Fig. 1). As the cutter advances along the rock surface, the tangential and normal components of the force acting on the cutter are measured by a load sensor and a data acquisition system controlled by LabVIEW at a raw sampling frequency $f = 600$ Hz. With this system, forces are mesured with a precision of about 1 N over the entire range up to 4000 N.

(a) (b)

Figure 3: (a)Wombat and (b) Metal holder.

The measurement spatial resolution

$$\lambda = \frac{2V}{f}, \tag{1}$$

where V is the cutter velocity and $f/2$ is the Nyquist frequency, represents the minimum distance over which the force variation can be accurately measured. With the cutter velocity ranging between 5 mm/s and 30 mm/s and the sampling frequency set at $f = 600$ Hz, the spatial resolution λ varies between 0.017 mm to 0.1 mm. As we ignore here stochastic events that occur at a length scale smaller than the grain size, the force signal is re-sampled with a spatial resolution of 0.1 mm, independent of the cutter velocity.

In order to capture the rock failure phenomenon, the entire cutting process was recorded with a camera (iPhone 11) attached to the vertical frame of the moving cart, see Fig. 3a. The camera is thus stationary relative to the cutter and has an acquisition rate of 60 and 240 frames per second (FPS) for the normal and slow-motion recording modes, respectively. Since previous studies have shown that the cutter velocity has negligible effects on the force response and on the rock chipping process [5, 31, 38], the cutter velocity is set to be 12 mm/s to facilitate the synchronization between the force signals (re-sampled at a resolution of 0.1 mm) and the recorded videos. The cutter traveling distance between two adjacent images is thus 0.2 mm for the normal videos, and is 0.05 mm for the slow-motion videos.

2.2. Rock Sample Preparation

The scratch tests were conducted on three rocks: Bonne Terre Dolomite (BTD), Alabama Marble (AM), and Dunnville Sandstone (DS). Samples without apparent

Rock Type	Density (g/cm^3)	UCS (MPa)	Tensile Strength (MPa)	Young's Modulus (GPa)	Toughness ($MPa\sqrt{m}$)
Bonne Terre Dolomite	2.5	172	8.5	24.3	1.6
Alabama Marble	2.73	123	5.1	24.8	1.13
Dunnville Sandstone	1.85	43	2.0	7.9	0.18

Table 1: Rock properties.

cracks or other damage were chosen for the experiments. The rock properties are listed in Table 1. The rock slab specimens were prepared as follows. First, a cubic rock block with a side length of 300 mm was sawn into several small cuboids with a squared cross section of 300 mm $\times$ 300 mm and a height of 45 mm. Then the small cuboids were sawn into rock slabs with a length of 300 mm, a width of 9.5 mm and a height of 45 mm. Small deviations in slab width and height were unavoidable due to weak vibrations of the saw. The rock slabs were then gradually ground to a final thickness of 9.0 mm within $\pm$0.1 mm along both the length and the height of the slab. Since water was used when sawing and grinding the rock, the samples were placed in a dryer at 150 °C for 24 hours and then kept in air for at least 24 hours before being used for the scratch tests.

2.3. Test Procedure

The depth of cut varied between 0.1 and 2.6 mm with increments of 0.05 mm from 0.1 to 0.5 mm, of 0.1 mm from 0.5 to 1.0 mm, and of 0.2 mm between 1.0 and 2.6 mm. This range of depth of cut covers the three regimes of failure: ductile, fragmentation, and brittle with increasing d. Tests at each depth of cut were repeated at least 3 times to minimize the influence of rock heterogeneity and to accumulate enough macro-cracking events. Since the focus of this research is the study of the brittle failure mechanisms, emphasis is thus placed on conducting the experiments in the fragmentation and the brittle regimes.

When a new slab was fixed in the holder, several preliminary leveling cuts at shallow depth of cut were done prior to testing in order to ensure a flat horizontal plane throughout the entire slab length. Additional leveling cuts are also needed after a testing cut conducted in the fragmentation or the brittle regime, to prepare the slab for the next test by removing the damaged rock below the surface. In the fragmentation regime, several leveling cuts are carried out with the total leveling depth of cut not smaller than the testing depth of cut, while in the brittle regime,

leveling cuts are required after each cut to smoothen the surface punctuated by small craters and irregular remnants caused by chipping. For each test, the tangential and normal force components were acquired by the force measuring system, while the cutting process was recorded by a camera for the entire duration of the test.

3. Classification of the Cutting Regimes

The rock failure regimes observed in the slab scratch tests depend on the depth of cut. As indicated earlier, there are three distinct regimes: ductile ($d_0 \leq d \leq d_*$), fragmentation ($d_* \leq d \leq d_{**}$), and brittle ($d_{**} \leq d$). While the lower limit in the ductile limit $d_0 = 0.1$ mm is set by technological constraints of the scratcher (in particular the radius of curvature of the cutting edge on the PDC, which is about 30 μm), the depths of cut d_* at the ductile/fragmentation transition and d_{**} at the fragmentation/brittle transition depend on the rock mechanical properties. In grained rocks, the physical lower limit of the depth of cut for the ductile regime, d_d, is likely to correspond to the mean grain size. Thus $d_d = O(0.1)$ mm for medium grained sandstone, but $d_d = O(0.001)$ mm for a shale

Observations of the rock failure in each regime can be summarized as follows.

- In the ductile regime, rock failure is associated with a continuous plastic flow of pulverized rock accumulated ahead of the cutter face. The rock failure process is mainly characterized by grinding or continuous de-cohesion of the constitutive matrix and grains.

- The fragmentation regime is characterized mainly by the appearance of small thin flake-like chips. Powder-like debris are produced along with the formation of flake-like chips and also by cutter grinding after the flake-like chips is separated from the intact rock. The size and total volume of the flake-like chips gradually dominate as the depth of cut increases in the fragmentation regime. Previous experiments [11] have shown that the particle size distribution follows a power law over a significant range of sizes. Analysis of scratch data [11] and numerical simulations [14] suggest that $d^* \backsim (K_{Ic}/q)^2$, where K_{Ic} is the mode I toughness and q is the UCS. As will be discussed in Section 5, shear fractures actually dominate the rock failure process in the fragmentation regime, implying that mode II toughness K_{IIc} could be a more relevant parameter, but also recognizing that the ratio K_{IIc}/K_{Ic} is commonly considered to be constant for rocks.

	Ductile regime	Fragmentation regime	Brittle regime
AM	$0.1 \backsim 0.5$ mm	$0.5 \backsim 2.0$ mm	$2.0 \backsim 3.0$ mm
BTD	$0.1 \backsim 0.3$ mm	$0.3 \backsim 1.4$ mm	$1.4 \backsim 3.0$ mm
DS	$0.1 \backsim 0.5$ mm	$0.5 \backsim 2.6$ mm	$2.6 \backsim 3.6$ mm

Table 2: Ranges of depth of cut for different cutting regimes for three types of rock.

- In the brittle regime, failure is associated with crack propagation. The cracks that have initiated around the cutter tip could either directly propagate upwards to the free surface, resulting in the formation of large flake-like chips and hence a slant surface, or first propagate sub-horizontally in an opening mode and then curve upward to the free surface, leading to chunk-like chips and a relatively flat surface. At times, the sub-horizontal crack just stops to propagate and the rock beam formed between the sub-horizontal crack and the free surface is crushed by the cutter as it advances. In rare circumstances, the crack propagates downwards and causes a complete splitting of the slab specimen. After a large piece of rock chip is removed, the depth of cut is effectively zero or close to zero and progressively increases until a new chip is formed, during which a small amount of powder-like cuttings is created.

The three cutting regimes can be classified not only according to the observed rock failure characteristics during cutting, but also to the scaling of the specific energy with the depth of cut. Figure 4 presents the log-log plots of the variation of the specific energy versus the depth of cut for tests on the three rocks (BTD, AM and DS). Indeed, these results show that the specific energy ϵ is independent of the depth of cut d in the ductile mode and follows a power law with an exponent of $-1/2$ in the fragmentation regime. Note that the transition from the ductile mode to the fragmentation mode is sharp for the DS and the BTD, but is gradual for the AM. In the brittle regime, the specific energy is inversely proportional to the depth of cut for the AM and the DS, noting that a consistent rock chipping pattern can be observed in these tests. In contrast, as will be discussed below, the chipping pattern is inconsistent when cutting the BTD, presumably due to its strong heterogeneity. This results in an apparent random variation of the specific energy with the depth of cut, which is exacerbated by the limited number of chipping events due to the short scratch length of order $O(10)$ cm. The ranges of depth of cut for different cutting regimes for the three rocks are listed in Table 2.

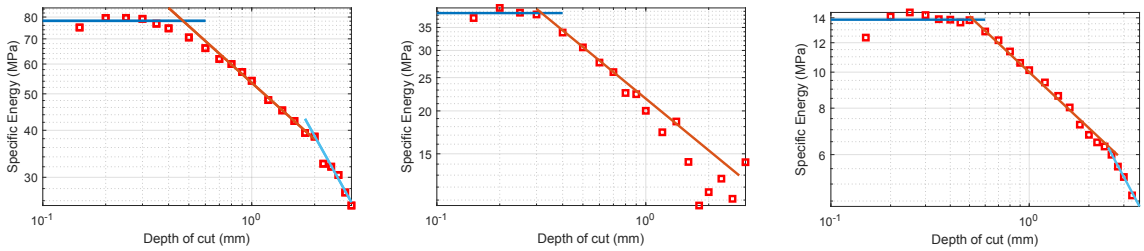

Figure 4: Scaling law of the specific energy versus the depth of cut for three cutting regimes: (a) Alabama Marble, (b) Bonne Terre Dolomite and (c) Dunnville Sandstone.

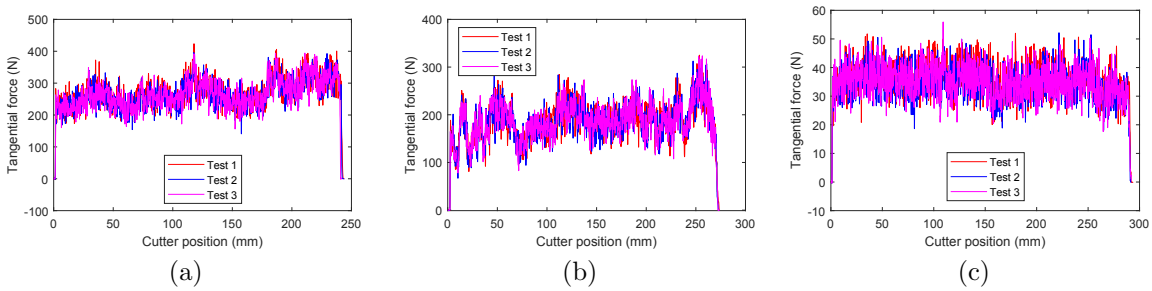

Figure 5: Variation of the tangential force signals for: (a) Alabama Marble, (b) Bonne Terre Dolomite, and (c) Dunnville Sandstone at a depth of cut of 0.2 mm with a spatial resolution of 0.1 mm.

4. Assessment of the Rock Heterogeneity

Extensive laboratory testing has led to the conclusion that the specific energy ϵ in the ductile regime does not depend on the depth of cut and that ϵ is well correlated with the rock UCS [9, 38, 39]. Furthermore, one of the benefits offered by the scratch test is that the cutting force signal bears information on the spatial variation of rock strength [9]. Figure 5 shows the cutting force signals at a depth of cut of 0.2 mm for the three tested rocks. This depth of cut ensures that cutting takes place in the ductile regime for each rock, see Table 2. The consistent trend of the cutting force variation among three tests reveals reproducible signal patterns, implying that the local rock strength determines the amplitude of the force signal for the three rocks.

The spatial variation of the cutting force signal in the ductile regime suggests that rock heterogeneity can be assessed at a resolution of about one centimeter. This can be done by applying a low-pass filter with a cutoff frequency on the original signals. The filtering operations are carried out by using the technique of maximum

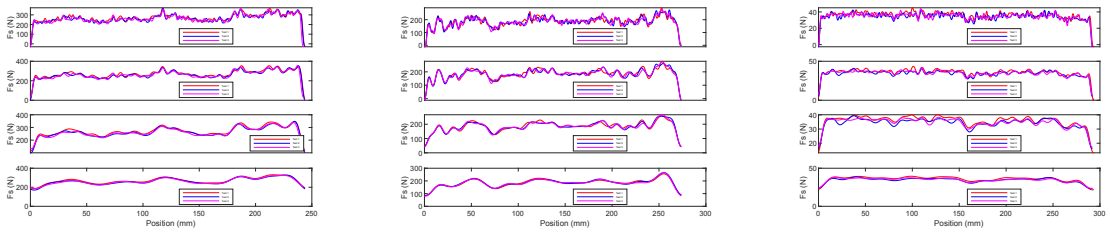

(a) (b) (c)

Figure 6: Successive filtering applied to the cutting force signals for: (a) Alabama Marble, (b) Bonne Terre Dolomite, and (c) Dunnville Sandstone with a reducing cutoff frequencies. The cutoff frequencies from the top plot to the bottom plot are 3.75 Hz, 1.88 Hz, 0.94 Hz and 0.47 Hz, which correspond to a length scale larger than 3.2mm, 6.38 mm, 12.76 mm, and 25.52 mm, respectively.

overlap discrete wavelet transform (MODWT) to decompose the initial signal into different frequency levels [40]. Increasing the level of decomposition thus corresponds to reducing the cutoff frequency, which is equivalent to increasing the measurement length scale at which the signal is observed.

Figure 6 shows the results of successive filtering operations with decreasing cutoff frequencies on the initial force signals in Fig. 5 for the three tests. The decomposition level used in MODWT is 4, 5, 6 and 7 from the top row of plot to the bottom row of plot in Fig. 6. Since the re-sampling frequency for the initial signal is 120 Hz, the corresponding cutoff frequencies are 3.75 Hz, 1.88 Hz, 0.94 Hz, and 0.47 Hz, indicating that the length scale over which the signals are observed are larger than 3.2 mm, 6.38 mm, 12.76 mm, and 25.52 mm, respectively. As shown in Fig. 6, decreasing the cutoff frequency wipes out the high-frequency details and leads to a good repeatability for the signals obtained at the same depth of cut.

Rock heterogeneity is inferred from the variation of rock strength along the cut. Since the filtered signal with a cutoff frequency of 0.94 Hz produces a good repeatability, it will be used to assess the level of rock heterogeneity. The coefficient of variation, i.e., the ratio of the standard deviation of the filtered signal to its mean, is used to characterize the level of rock heterogeneity at the scale of the samples used for the scratch tests. The averaged values of the coefficient of variation for the three tests on the BTD, the AM, and the DS are 0.169, 0.126, and 0.089, respectively. This suggests that the DS has the lowest level of heterogeneity while the BTD has the highest level of heterogeneity.

(a) (b) (c)

Figure 7: Characteristics of rock failure in the fragmentation regime for: (a) Alabama Marble at a depth of cut 0.8 mm, (b) Bonne Terre Dolomite at a depth of cut of 0.6 mm and (c) Dunnville Sandstone at a depth of cut of 1.2 mm.

5. Fragmentation Regime

The fragmentation regime has not received enough attention in previous rock cutting studies, even though both Richard [8] and Chaput [10] reported the existence of a transition regime characterized by the formation of smaller secondary rock chippings. A review of the recorded videos taken during scratch tests on the BTD, AM and DS reveals that both powder-like debris and thin flake-like fragments are formed when the depth of cut is in the fragmentation regime, see Fig. 7. The size and the volumetric proportion of the thin-flake fragments increases with the depth of cut, as shown in Fig. 8, where the cuttings from tests on the three rocks in the fragmentation regime are compared at three depths of cut.

The consistent thin flake-like morphology of the fragments created in the transition regime indicates that the same failure mechanism dominates the fragmentation regime. This is confirmed by an examination of the fracture surface of the thin flake-like fragments using a Scanning Electron Microscope (SEM), see the photographs in Fig. 9 for the BTD and the AM. These images show similar characteristics, i.e., the fracture surface has a rough appearance resulting from grain breakage along the crystalline boundary or within a grain. Since the cutter used in the scratch test has a positive rake angle, the rock is subject to a compressive stress field, which causes the interaction and propagation of a system of micro-cracks and the formation of thin flake-like fragments. Moreover, it is commonly observed that a slant surface was created after the fragments were expelled ahead of the cutter, as shown in Fig. 10. This suggests that the formation of the thin flake-like fragments is caused by shear fractures.

Figure 11 illustrates the tangential force signals corresponding to the cutting process shown in Fig. 7. The force signals are characterized by a saw-tooth pattern with a small spread between peaks, reflecting the observed repetitive fragmentation

Figure 8: Collection of the rock cuttings for: (a) Alabama Marble, (b) Bonne Terre Dolomite and (c) Dunnville Sandstone, each at three different depths of cut.

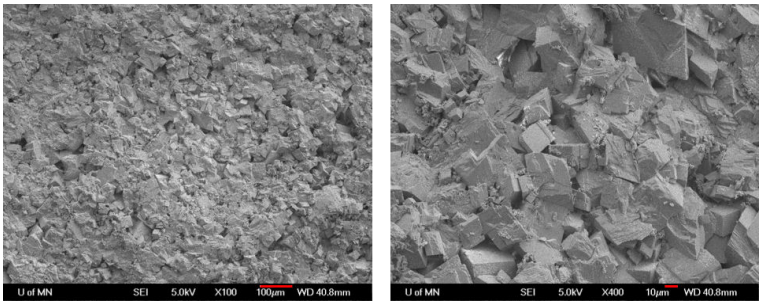

(a)

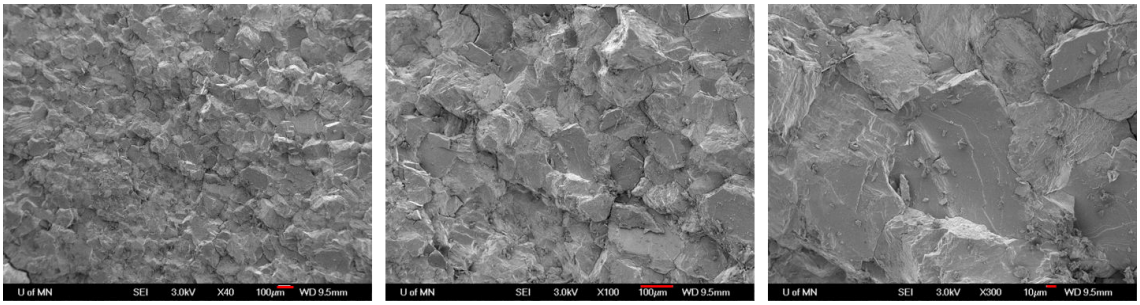

(b)

Figure 9: Images of the fracture surface of flake-like fragments obtained with a Scanning Electron Microscope for cutting tests conducted on (a) Bonne Terre Dolomite at a depth of cut of 1.0 mm and (b) Alabama Marble at a depth of cut of 2.0 mm.

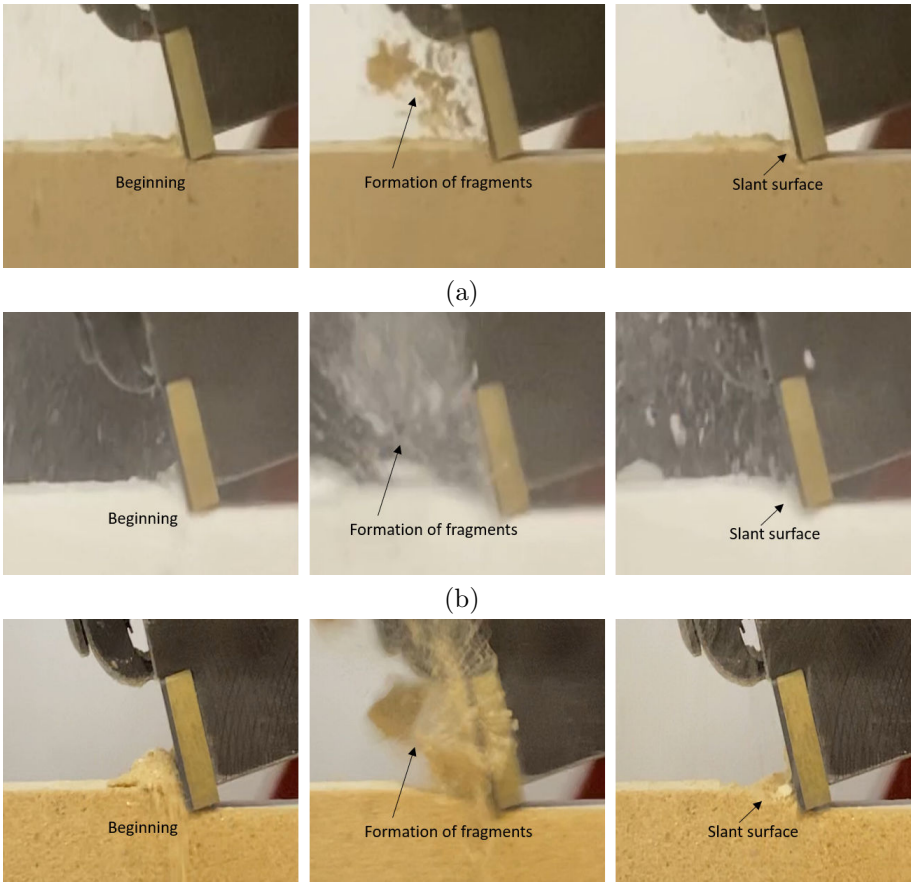

Figure 10: A series of snap shots showing the formation of a slant surface after the fragments were ejected ahead of the cutter for cutting on (a) Bonne Terre Dolomite at a depth of cut of 1.0 mm, (b) Alabama Marble at a depth of cut of 1.6 mm, and (c) Dunnville Sandstone at a depth of cut of 1.8mm.

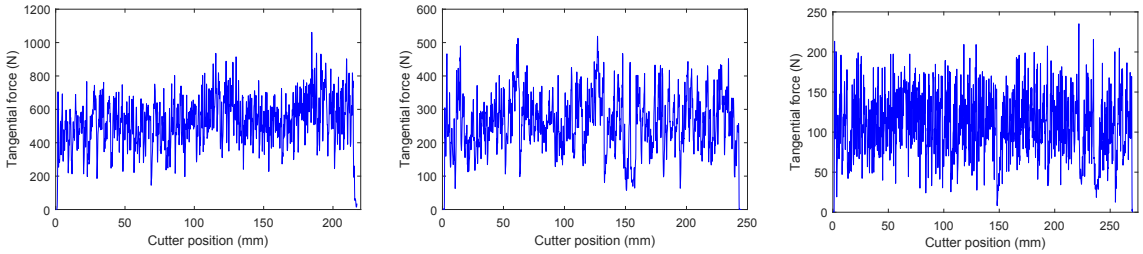

(a) (b) (c)

Figure 11: Typical tangential force signals for: (a) Alabama Marble at a depth of cut 0.8 mm, (b) Bonne Terre Dolomite at a depth of cut of 0.6 mm and (c) Dunnville Sandstone at a depth of cut of 1.2 mm with a resolution of 0.1 mm.

process. The force ascent stage is related to loading the rock by the cutter whereas the force descent stage is associated with rock breakage. The cutting force value seldom reaches zero, implying that the cutter is in contact with the rock over the entire cutting process. It is also observed that the cutting force fluctuations as well as the spread between peaks increase with the depth of cut, a consequence of larger fragments being created at larger depth of cut.

6. Brittle Regime

6.1. Characteristics of the Brittle Failure

Difference in the failure mode between the BTD, AM and DS appears when cutting takes place in the brittle regime. A review of the videos recorded when testing the three rocks indicates three types of chipping patterns:

- Shear-induced chipping. Flake-like chips still dominate the rock cuttings in the brittle regime for the AM and the DS. Similar to the fragmentation regime, rock failure is characterized by the rapid formation of large chips and the subsequent ejection of the chips ahead of the cutter at high speed. An emission of sudden sound accompanies the chipping process. A slant free surface is created after the large rock chip breaks off from the virgin rock (see Fig. 12a).

- Tensile fracture chipping. The initiation and propagation of tensile macrocracks were commonly observed when cutting the BTD (see Fig. 12b), but is rarely observed when cutting the AM or the DS. The tensile crack first remains sub-parallel to the free surface and then propagates upward, leading to the formation of chunk-like chips. The averaged crack length increases with the depth of cut.

- Surface instability. The chipping pattern results from the propagation of surface-parallel cracks close to the free surface. The rock between the surface-parallel crack and the free surface can be treated as a beam under compressive loads exerted by the cutter. As the critical compressive stress is reached, loss of stability due to buckling of the surface leads to the crack propagation and eventually to rock breakage in the middle of the rock beam (see Fig. 12c).

Typical cutting force signals for the BTD, the AM and the DS in the brittle regime are illustrated in Fig. 13. The sections marked by the dotted red line in Fig. 13a indicate regions where the forces are close to zero, a result of chipping caused by the propagation of tensile cracks when cutting the BTD. The force signals for the AM and the DS follow a saw-tooth pattern but with a large variation of the force magnitude caused by the propagation of a system of microcracks, as shown in Figs. 13b and 13c, respectively.

6.2. Fracture Mechanisms

Despite a significant amount of work done over the past a few years, the nature of the fracture mechanisms involved in the scratch tests remains somewhat elusive. Observations from recorded videos together with evidence of two different types of chip morphology suggest that there exists different fracture mechanisms responsible for the chipping process. It is hypothesized that the flake-like chips result from the shear fractures induced by the compressive load imposed by the cutter motion. In contrast, the formation of chunk-like chips is apparently associated with the propagation of a tensile crack as shown in Fig. 12b.

Figure 14 shows the SEM images of the fracture surface for both flake-like and chunk-like chips obtained at the same depth of cut of 2.0 mm when cutting on the BTD. These chips were collected carefully. We first recorded the cutting process and left the cuttings untouched after the test, and then reviewed the recorded videos to track the trajectory of one flying chip so as to identify its origin and failure pattern. It is thus confirmed that the flake-like and chunk-like chips are, respectively, created by the propagation of shear and sub-horizontal tensile cracks, see Figs. 15 and 12b corresponding to the formation of flake-like and chunk-like chips, respectively.

It can be seen from Fig. 14 that the fracture surface of the flake-like chip has a rough appearance that is similar to the one shown in Fig. 9, suggesting that the formation of flake-like chips in both the fragmentation and the brittle regimes is caused by the same failure mechanism. On the other hand, the fracture surface of the chunk-like chips has a smoother appearance in comparison with the flake-like chips. This drastic difference is consistent for all the specimens observed with the SEM; that is, the chunk-like chips have smooth fracture surface whereas the flake-like

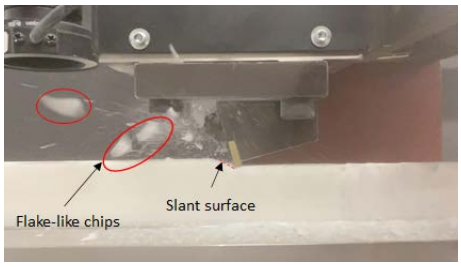

(a)

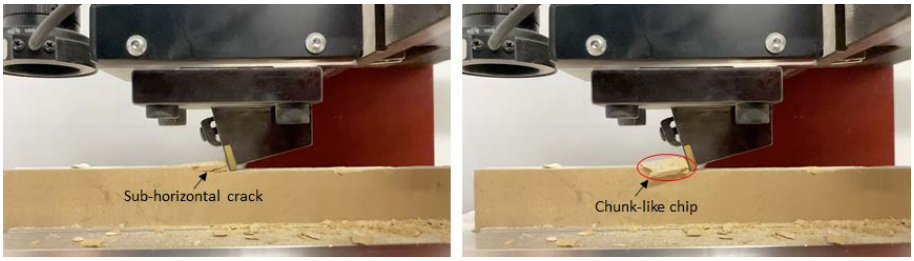

(b)

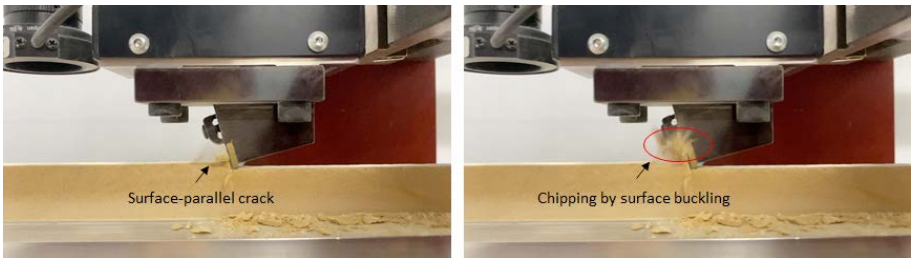

(c)

Figure 12: Characteristics of chipping patterns in the brittle regime for: (a) shear-induced chipping on Alabama Marble at a 2.6 mm depth of cut, (b) tensile fracture chipping on Bonne Terre Dolomite at a 2.0 mm depth of cut, and (c) surface instability on Dunnville Sandstone at a 2.6 mm depth of cut.

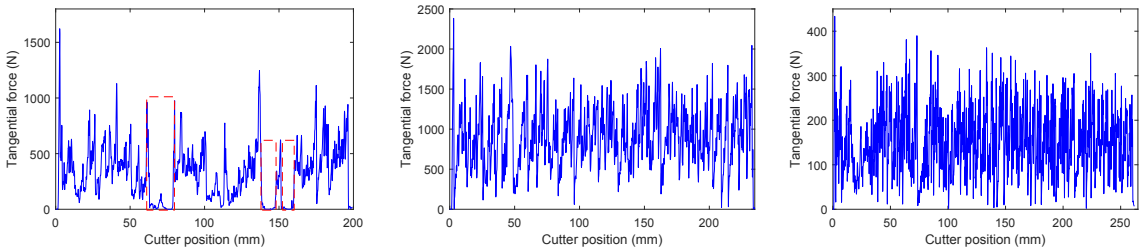

(a) (b) (c)

Figure 13: Examples of the tangential force signals for: (a) Bonne Terre Dolomite at a 2.3 mm depth of cut, (b) Alabama Marble at a 2.6 mm depth of cut, and (c) Dunnville Sandstone at a 2.6 mm depth of cut with a spatial resolution of 0.1 mm.

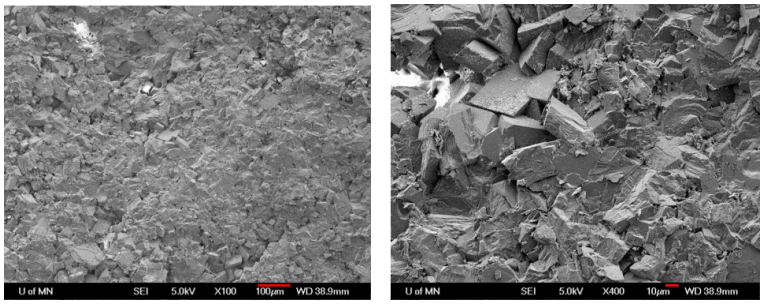

(a)

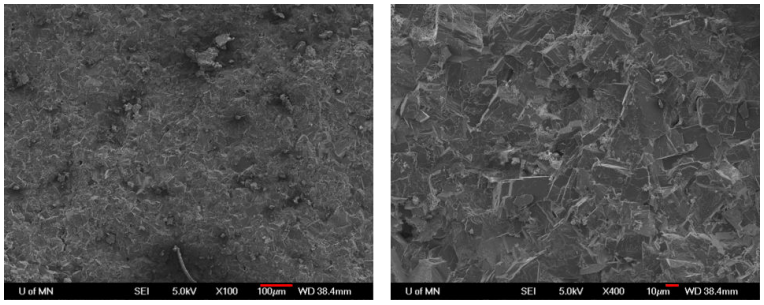

(b)

Figure 14: SEM images of the fracture surfaces of (a) a flake-like and (b) a chunk-like chip obtained from cutting the BTD at a 2.0 mm depth of cut. The scales used for the left and right pictures are 100 μm and 10 μm, respectively.

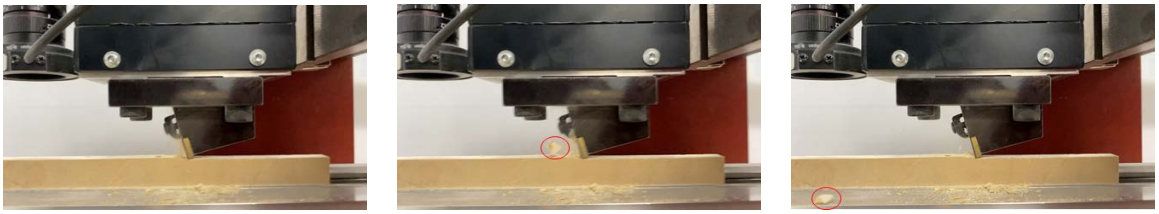

Figure 15: Identification of the formation for flake-like fragments at a depth of cut 1.0 mm via reviewing the recorded videos. The flake-like chip is marked by the red circle.

chips have rough fracture surface, independent of the rock material and the depth of cut. It is thus reasonable to hypothesize that two different failure mechanisms exists in the rock chipping process. Since the formation of a chunk-like chip is closely related to the propagation of a tensile macrocrack (see Fig. 12b), the formation of flake-like chips is postulated to be caused by shear fractures. The growth of these fractures occur too rapidly to be observed at the maximum 240 FPS used in the recorded videos.

In contrast, the stable propagation of a tensile crack can readily be captured in the recorded videos. As an example, the propagation of the tensile crack shown in Fig. 12b is captured via a series of snap shots presented in Fig. 16. By noting that the depth of cut is 2.0 mm, the final crack length can be estimated to be about 8.0 mm. Since the time interval between two adjacent frames for a slow-motion video is 0.0042 s, the averaged propagation velocity of this sub-horizontal crack is thus about 0.48 m/s. On the other hand, the shear-induced crack always occurs within one frame such that its propagation is hardly observed. For the flake-like fragments shown in Fig. 15, its length can be estimated to be 4.8 mm based a depth of cut of 1.0 mm. The averaged shear-induced crack propagation speed should thus be larger than about 1.2 m/s. The different fracture surface appearances between the chunk-like and the flake-like chips could possibly be explained by the different propagation speeds between the shear and the tensile cracks.

Based on the above analysis, the main rock failure mechanism in the fragmentation regime is the shear fracture since flake-like chips dominate in this regime for each rock. The failure mechanism remains shear-induced fracture for the AM and the DS in the brittle regime, but is a combination of shear and tensile crack for the BTD in the brittle regime.

6.3. The Crushed Zone

It has been proposed that the presence of a crushed zone ahead of the cutter with a positive rake angle provides a mechanism by which tensile cracks are initiated in

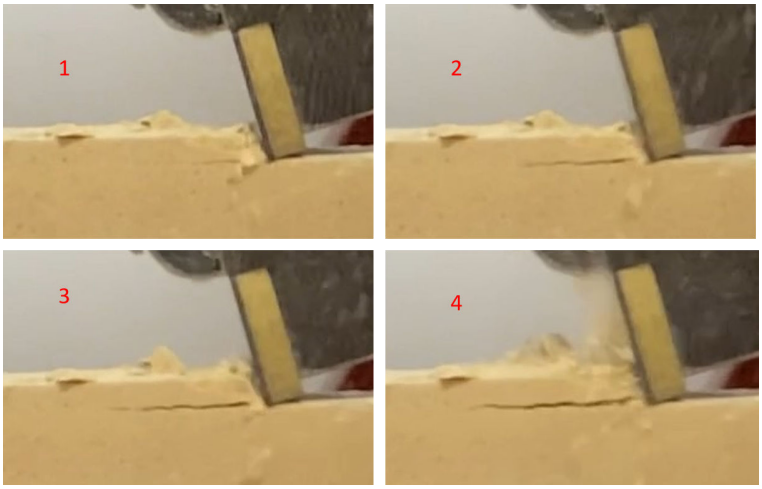

Figure 16: Illustration of the propagation of a sub-horizontal crack when cutting on the Bonne Terre Dolomite at a 2.0 mm depth of cut.

the rock under a compressive stress field [8, 17, 29, 36]. Moreover, the dominance of tensile or shear fracture is closely related to the geometrical shape of the crushed zone surrounding the tool tip, which acts as a wedge to initiate a tensile crack [35, 37]. The formation of a crushed zone as a precursor to the initiation of a tensile crack has been confirmed by several experimental studies using imaging methods [29, 35, 36].

The rock in the crushed zone is pulverized into powders due to the high stress concentration at the cutter tip. The rock powder is re-compacted by the cutter and then adheres to the trailing edge of the rock chips, as they break off from the virgin rock when the crack propagates to the free surface [32]. Therefore, the powdery appearance at the trailing edge of a chunk–like chip serves as evidence for the formation of a crushed zone. Such evidence was commonly observed in the BTD rock chips resulting from tensile crack propagation, as shown in Fig. 17. It is clearly seen from the left picture in Fig. 17 that there is a powdery appearance at the trailing edge of a rock chip, which was then put back in place in the right picture of Fig. 17, suggesting that the powdery region is just at the cutter tip. This further indicates that the crushed zone is formed near the cutter tip due to the compressive stress concentration. Powdery appearance was also observed in other chunk-like chips at their trailing edge.

On the other hand, compression of the rock in the crushed zone causes the breaking of small fragments on the sides of the slab near the cutter tip. This also provides evidence for the formation of a crushed zone [36]. Figure 18 presents a series of snap shots, which clearly show the expulsion of a small fragment ahead of the cutter tip

Figure 17: Powdery appearance at the trailing edge of a rock chip as evidence for the formation of the crushed zone at the cutter tip.

(see the first three consecutive images in Fig. 18) and the subsequent tensile crack caused by the wedging action (see the fourth image in Fig. 18).

A careful review of the recorded videos and inspection of the flake-like chips without powdery appearance at the chip trailing edge indicate that the crushed zone is not formed in the creation of flake-like chips. It is thus reasonable to conclude that the initiation of the tensile crack follows the formation of the crushed zone whereas the shear fracture occurs in the absence of the crushed zone, which agrees with previous observations [35].

For the BTD, the formation of the crushed zone in the brittle regime is more commonly observed than in the fragmentation regime, implying that the depth of cut affects the formation of the crushed zone. The contact condition between the cutter and the rock also have an influence on the formation of the crushed zone since the tensile cracks are more likely to appear when the cutter and the rock are in partial contact, which amplifies the stress concentration at the cutter tip and thus facilitates the formation of the crushed zone. The fact that the crushed zone is absent when cutting the AM and the DS but present when cutting the BTD indicates that the rock properties, such as porosity, mineral composition and grain size, also have effects on the size of the crushed zone.

When cutting the BTD in the brittle regime, it is observed through a review of the recorded videos that the length of the sub-horizontal cracks increases with the depth of cut while the number of the tensile fracture events remains almost constant. The number and length of the sub-horizontal crack were measured for the tests at the same depth of cut. Figure 19 shows that the averaged crack length has a linear relationship with the depth of cut, with the error bar indicating the standard deviation.

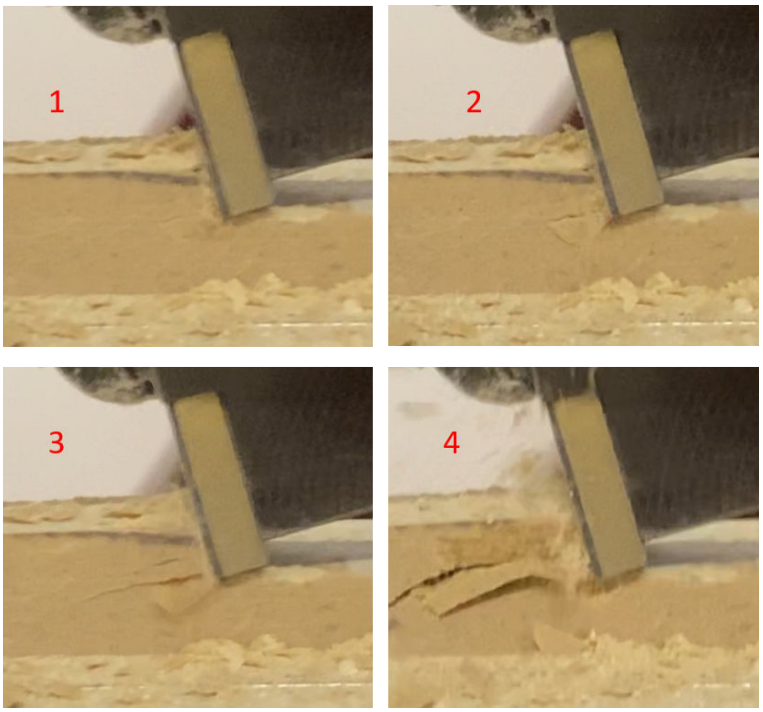

Figure 18: Illustration of the expulsion of small fragments as evidence for the formation of the crushed zone.

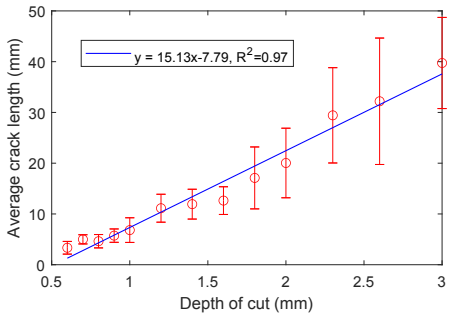

Figure 19: Average crack length versus the depth of cut for cutting tests on the Bonne Terre Dolomite. The error bar corresponds to the standard deviation.

6.4. Analysis of Different Chipping Patterns via Synchronization

Analysis of the cutter-rock interaction is usually based on an examination of the cutting force. In previous research, only average values or average peak values of the cutting force were assessed to study the effects of various factors, such as depth of cut, rake angle, cutter speed, etc., on the cutting response. Investigation on the rock failure process by analyzing the fluctuations of the cutting force has been recently reported in [41, 42]. It has been shown that the fluctuations have a close relationship with the rock failure mode and can be used to quantitatively describe rock failure.

As a complementary approach to gain a better understanding of the cutting process, high-speed filming has been employed to capture the rock chipping phenomena in previous studies [26, 31, 35, 43]. However, to our best knowledge, the recorded videos have not been synchronized with the force signals. As shown below, such a synchronization provides valuable information regarding the relationship between the cutting force and the rock failure process.

As mentioned in Subsection 2.1, the sampling interval of the force signals is 0.1 mm and the cutter traveling distance between two adjacent photographs is 0.05 mm for a slow-motion recording mode. This relationship makes the synchronization between the force signals and the recorded videos readily to be carried out in this study. Therefore, the chipping patterns caused by tensile crack propagation, shear fracture and surface instability were analyzed by synchronizing the force signal and recorded videos.

The most obvious chipping pattern in the brittle regime results from the initiation and propagation of a tensile macrocrack. Figure 20a shows a typical cutting force variation corresponding to the propagation of a tensile macrocrack. This event is divided into 6 stages as marked in Fig. 20a. Through the synchronization, six snap shots corresponding to the six stages of force variation are presented in Fig. 20b. A slant free surface resulting from previous chipping action can be seen in the first image such that the force amplitude increases in the first stage due to the gradual increase of the actual depth of cut as the cutter moves along this slant surface. The force drop in the second stage corresponds to the formation of a small amount of fragments as shown in the second image. This is caused by the interaction and coalescence of microcracks under the action of compressive loads exerted by the cutter. After the ejection of the fragments ahead of the cutter, the third image shows that the cutter is in full contact with the rock and starts to compress the rock as the cutter travels in the third stage. The force drop in the fourth stage corresponds to the propagation of a tensile crack, as shown in the fourth image. Accompanying the appearance of the tensile crack is the formation of small fragments, which come from two sources. First of all, propagation of a tensile crack reduces the loading capacity of the rock

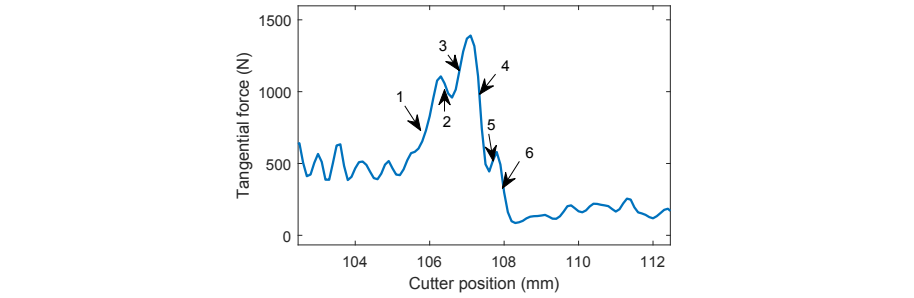

(a)

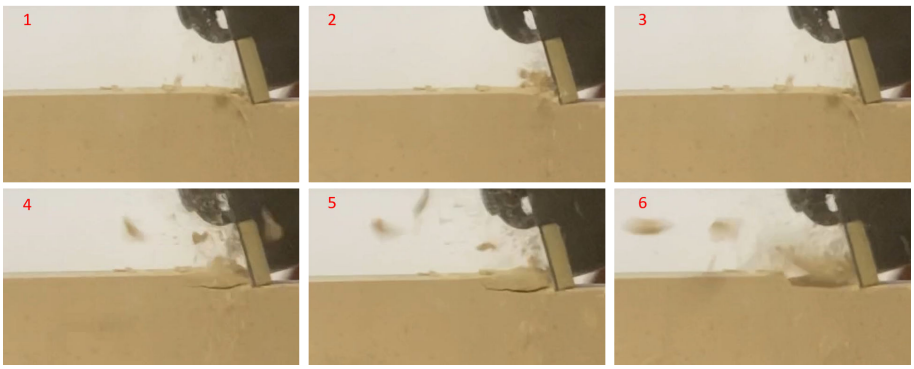

(b)

Figure 20: Illustration of the tensile fracture failure: (a) the force variation and (b) snap shots that corresponds to the evolution of a tensile macrocrack. Test performed on the Bonne Terre Dolomite at a depth of cut of 2.0 mm.

beam such that a small amount of the rock ahead of the cutter is fragmented by the compressive load. Other fragments are expelled on both sides of the rock slab ahead of the cutter tip, a consequence of the formation of the crushed zone. The fifth image suggests that the slight increase of the force in the fifth stage is associated with a sub-horizontal tensile crack propagating upward to the free surface, possibly implying the transition from a tensile to a shear crack. The force drop in the final stage is because of the breaking off of the rock chip, as illustrated in the sixth image.

Even though tensile macrocracks can be visualized by naked eyes, the most common chipping pattern from the review of the recorded videos is actually the shear fracture, leading to the formation of flake-like chips. Figure 21a shows the force variation for two cases of shear-induced fracture with the corresponding snapshots shown in Fig. 21b for case 1 and in Fig. 21c for case 2. As can be seen from Fig. 21a, both cases consist of a force ascending stage and a force dropping stage with a steep slope. The first images in both Figs. 21b and 21c correspond to the peak values for both

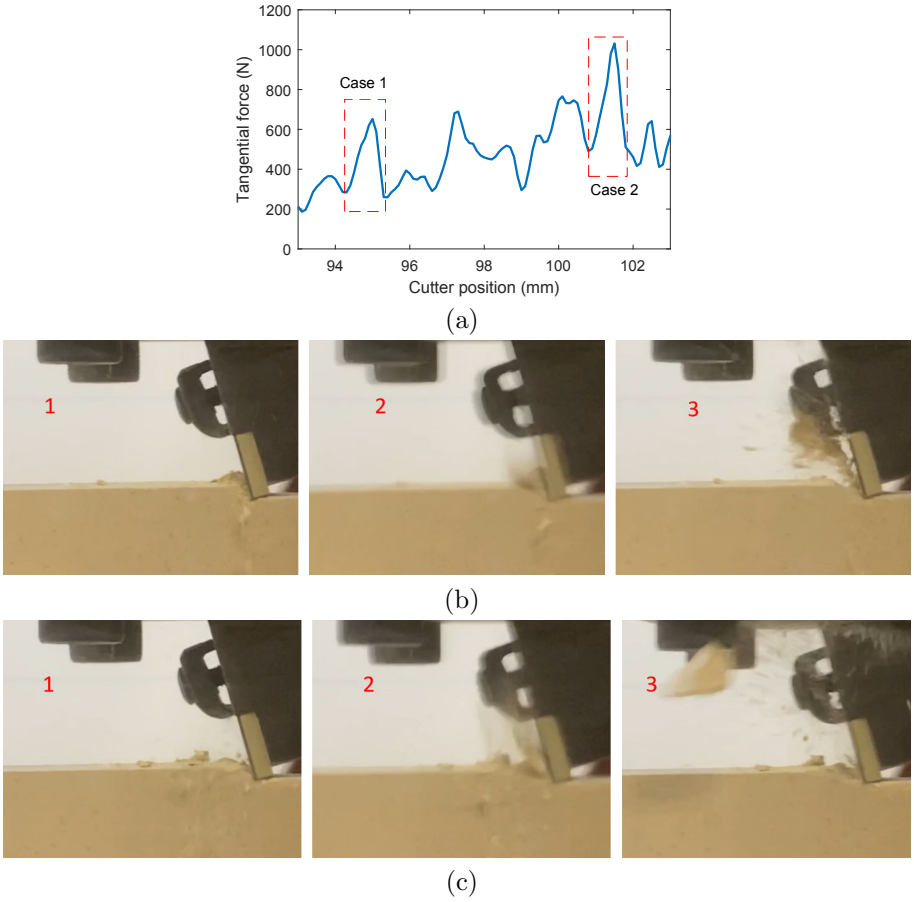

Figure 21: Illustration of two cases of shear-induced failure: (a) the force variation and (b) snap shots for the first case , and (c) snap shots for the second case. Test performed on the Bonne Terre Dolomite at a depth of cut of 2.0 mm.

cases and the second ones are the adjacent subsequent frames. The time interval of 0.0042 s between two adjacent frames reveals the shear-induced failure occurs quite rapidly. The third images in Figs. 21b and 21c show the formation and ejection of flake-like chips just ahead of the cutter face, resulting in a slant free surface.

Figure 22a presents the force variation of two cases of surface instability-related chipping. Three consecutive snap shots that correspond to cases 1 and 2 are shown in Figs. 22b and 22c, respectively. The first images in Figs. 22b and 22c correspond to the peak force values for case 1 and case 2, respectively. The peak force values are believed to be determined by the vertical distance between the surface-parallel crack and the free surface. The vertical distance for case 1 is larger than that for

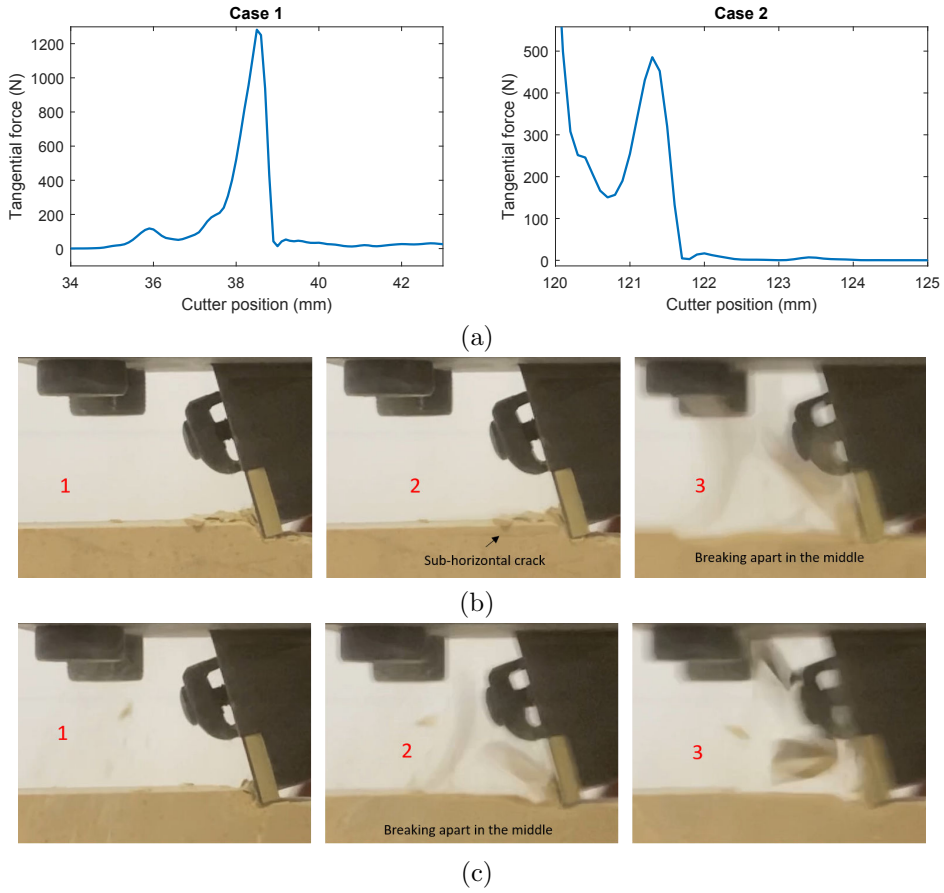

Figure 22: Illustration of two cases of surface-instability-related failure: (a) the force variation, (b) snap shot for the first case, and (c) snap shots for the second case. Test is performed on the Bonne Terre Dolomite at a depth of cut of 2.0 mm.

case 2 as can be seen from the comparison between the third image in Fig. 22b and the second image in Fig. 22c. The propagation of the surface-parallel crack was captured in the second image in Fig. 22b, which led to the rock chipping illustrated in the third image in Fig. 22b. The characteristic of the surface instability-induced chipping is that the rock beam breaks off into two chunk-like chips in the middle because of buckling, as shown in the second and third images in Fig. 22b. The consecutive images in Figs. 22b and 22c imply that the surface instability-related chipping occurs rapidly with a sharp force drop as shown in Fig. 22a.

7. Cutting Energy Partition

It has been assumed by several authors that energy in the brittle regime is essentialy dissipated in the creation of new surfaces associated with the propagation of a tensile macrocrack. Mathematical models based on this assumption have been proposed to study the transition depth of cut and to assess the rock fracture toughness [13, 17, 38, 44]. However, experimental observations from rock cutting tests suggest that the energy dissipated in the propagation of tensile crack is negligible when compared to other energy-consumption sources, such as the formation of the crushed zone and the heat energy due to friction [5, 33, 45, 46].

In the following, we analyze the energy partitioning in the rock cutting process in order to assess the validity of the above theoretical assumption. For this purpose, it is sufficient to consider one chipping event associated with propagation of a tensile crack, as shown in Fig. 20. Since the cutter moves horizontally parallel to the rock surface, the work expended in cutting the rock over the chipping event, W, can be estimated from the tangential force signal shown in Fig. 20 according to

$$W = \int_{x_0}^{x_0+\delta} F_s dx \tag{2}$$

where F_s is the tangential force, x_0 is the initial position of the cutter, and δ is the distance traveled by the cutter over the entire chipping period. The energy J_s used for creating the tensile crack surfaces shown in Fig. 20b can be calculated as

$$J_s = 2\gamma w L \tag{3}$$

where $\gamma = {K_{IC}^2}/{E}$ is the surface energy for a plane stress problem with E denoting the Young's modulus, w is the slab width, and L is the crack length that can be estimated from the recorded video.

According to the force signal in Fig. 20 and Eq. (2), the external work W in the third stage ($x_0 = 106.6$ mm and $\delta = 0.5$ mm), prior to the appearance of the tensile crack, is estimated to be 0.72 J. In contrast, the energy J_s dissipated in creating the tensile crack surfaces is estimated to be be about 10^{-3} J, according to the mechanical properties of the BTD in Table 1 and by noting the estimated crack length $L = 5.1$ mm (see the fifth image in Fig. 20b) and the slab thickness $w = 9$ mm. The energy dissipated in creating new tensile crack surface is thus two orders of magnitude smaller than the measured external work provided during the whole chipping event. The formation of powder-like and small flake-like fragments which accompany the propagation of a tensile crack, as seen from Fig. 20b, is thus expected to be the main contributor to the energy dissipation. This is consistent

with experimental evidence that the energy required to break intact rock into small fragments increases as the size of the fragments decreases [47, 48].

Other detectable energy-consumption sources in the rock cutting process include mechanical energy due to cutter vibration resulting from the force unloading, kinetic energy of the flying fragments, sound emission energy, heat energy due to friction among rock cuttings and between the rock and the cutter, etc.. The mechanical energy and kinetic energy of the flying fragments is estimated to be negligible, whereas the sound emission energy and heat energy cannot be estimated in our experiments. It is claimed by Linquist [45] that heat ultimately represents a major part of the total energy dissipated whereas the surface energy takes only $2\% - 3\%$ of the total energy in cutting hard rocks.

In summary, it appears that energy expended in creating the new surfaces associated with the formation of a chunk-like chip when cutting rock in the brittle regime is only a small fraction of the total external work, which is mainly consumed in the production of powder-like and flake-like fragments. Therefore, models on the based on assuming that the cutting energy is essentially dissipated in propagating a tensile macrocrack result in misleading conclusions.

8. Conclusions

Based on the slab scratch tests on three types of rock, this paper first classifies the rock failure modes into ductile, fragmentation and brittle modes according to the scaling law of the specific energy with respect to the depth of cut. Moreover, each mode is associated with different shapes of rock debris/fragments and different characteristics of the force signals, which are described as follows.

- Ductile regime. The dominant fragment shapes in the ductile regime is powder-like since the depth of cut is of the same order of the magnitude as the grain size. For homogeneous rocks, the cutting force signal resembles a white noise whereas the variation of the cutting force signal for heterogeneous rock is determined by the local rock strength. Application of a low-pass filter on the cutting force signals in the ductile regime is useful for the assessment of the rock heterogeneity.

- Fragmentation regime. Both powder-like and small thin flake-like fragments are created in the fragmentation regime. The size of the flake-like fragments increases with the depth of cut. The force signal presents a marked saw-tooth pattern with the spread between peaks increasing with the depth of cut, a consequence of the formation of larger fragments as the depth of cut increases.

- Brittle regime. Both flake-like and chunk-like chips were observed in the brittle regime. The formation of the chunk-like chips results from the propagation of tensile cracks. The force signal still presents a saw-tooth pattern but with intervals of force close to zero caused by the removal of rock ahead of the cutter due to the propagation of a tensile crack.

The fracture surfaces of the chunk-like and flake-like chips obtained with a Scanning Electron Microscope show appreciably different fractography, suggesting that two different fracture mechanisms exist in the rock cutting process. The chunk-like chips result from the tensile crack propagation whereas the flake-like chips are caused by shear fractures. The fragmentation regime is thus dominated by the shear-induced fracture for all three types of rock. However, for the brittle regime, the dominant failure mechanism remains shear-induced for the AM and DS, but is a combination of shear-induced fracture and tensile fracture for the BTD. Experimental observations show that the initiation of a tensile crack follows the formation of a crushed zone at the cutter tips, while the shear-induced fracture takes place in the absence of the crushed zone. Factors that affect the formation of the crushed zone include the depth of cut, contact condition between the cutter and the rock properties, such as the porosity, hardness and grain size, etc.

Synchronization between the force signals and the recorded videos provided detailed information regarding the force responses to the rock chipping process resulting from tensile crack propagation, shear-induced fracture and surface instability, respectively. With the help of the synchronization, the external work provided for a typical chipping event associated with the propagation of a tensile crack was calculated to be about two orders of magnitude larger than the energy used for creating new tensile crack surfaces. This invalidates the published models based on the assumption that most of the cutting energy is dissipated in creating new tensile crack surfaces in the brittle regime.

Data availability

Datasets containing cutting force signals, videos of rock cutting processes, particle size distribution from sieving analysis obtained from scratch tests conducted on different rocks are available for download from the Digital Conservancy site of the University of Minnesota: Alabama marble (https://hdl.handle.net/11299/228461), Dunnville sandstone (https://hdl.handle.net/11299/228463), Bonne Terre dolomite (https://hdl.handle.net/11299/228462), Burlington limestone (https://hdl.handle.net/11299/228464). Furthermore, datasets pertaining to UCS tests and indirect tensile tests for Alabama

Marble, Bonne Terre Dolomite, Burlington Limestone, and Dunnville Sandstone are also available for download (https://hdl.handle.net/11299/228460).

Declaration of competing interest

The authors declare that they have no known competing financial interests or personal relationships that could have appeared to influence the work reported in this paper.

Acknowledgments

The main funding for this research was provided by the National Science Foundation (Grant Number 1742823) Any opinions, findings and conclusions or recommendations expressed in this material are those of the authors and do not necessarily reflect the views of the National Science Foundation. The research was also partially supported by the Theodore W. Bennett Chair in Mining Engineering and Rock Mechanics. These supports are gratefully acknowledged.

[1] Evans I. A theory of the basic mechanics of coal ploughing. In: Mining Research. Elsevier; 1962. p. 761–798.

[2] Nishimatsu Y. The mechanics of rock cutting. In: International Journal of Rock Mechanics and Mining Sciences & Geomechanics Abstracts. vol. 9. Elsevier; 1972. p. 261–270.

[3] Deketh H, Grima MA, Hergarden I, Giezen M, Verhoef P. Towards the prediction of rock excavation machine performance. Bulletin of Engineering Geology and the Environment. 1998;57(1):3–15.

[4] Akbari B, Miska S, Yu M, Rahmani R. The effects of size, chamfer geometry, and back rake angle on frictional response of PDC cutters. In: 48th US Rock Mechanics/Geomechanics Symposium. OnePetro; 2014. .

[5] Che D, Zhang W, Ehmann K. Chip formation and force responses in linear rock cutting: An experimental study. Journal of Manufacturing Science and Engineering. 2017;139(1).

[6] Dagrain F, Detournay E, Richard T, et al. Influence of cutter geometry in rock cutting. In: DC Rocks 2001, The 38th US Symposium on Rock Mechanics (USRMS). American Rock Mechanics Association; 2001. .

[7] Richard T, Detournay E, Drescher A, Nicodeme P, Fourmaintraux D, et al. The scratch test as a means to measure strength of sedimentary rocks. In: SPE/ISRM rock mechanics in petroleum engineering. Society of Petroleum Engineers; 1998. .

[8] Richard T. Determination of rock strength from cutting tests. University of Minnesota; 1999.

[9] Richard T, Dagrain F, Poyol E, Detournay E. Rock strength determination from scratch tests. Engineering Geology. 2012;147:91–100.

[10] Chaput E. Observations and analysis of hard rock cutting failure mechanisms using PDC cutters. Imperial College of Science, Technology and Medicine; 1991.

[11] Peña C. An experimental study of the fragmentation process in rock cutting. University of Minnesota; 2010.

[12] Huang H, Detournay E. Intrinsic length scales in tool-rock interaction. International Journal of Geomechanics. 2008;8(1):39–44.

[13] Akono AT, Ulm FJ. Scratch test model for the determination of fracture toughness. Engineering Fracture Mechanics. 2011;78(2):334–342.

[14] Huang H, Lecampion B, Detournay E. Discrete element modeling of tool-rock interaction I: rock cutting. International Journal for Numerical and Analytical Methods in Geomechanics. 2013;37(13):1913–1929.

[15] Zhou Y, Lin JS. On the critical failure mode transition depth for rock cutting. International Journal of Rock Mechanics and Mining Sciences. 2013;62:131–137.

[16] He X, Xu C. Discrete element modelling of rock cutting: from ductile to brittle transition. International Journal for Numerical and Analytical Methods in Geomechanics. 2015;39(12):1331–1351.

[17] Liu W, Zhu X, Jing J. The analysis of ductile-brittle failure mode transition in rock cutting. Journal of Petroleum Science and Engineering. 2018;163:311–319.

[18] Zhou Y, Lin JS. Modeling the ductile–brittle failure mode transition in rock cutting. Engineering Fracture Mechanics. 2014;127:135–147.

[19] He X, Xu C, Peng K, Huang G. On the critical failure mode transition depth for rock cutting with different back rake angles. Tunnelling and Underground Space Technology. 2017;63:95–105.

[20] Akono AT, Reis PM, Ulm FJ. Scratching as a fracture process: From butter to steel. Physical review letters. 2011;106(20):204302.

[21] Akono AT, Ulm FJ. An improved technique for characterizing the fracture toughness via scratch test experiments. Wear. 2014;313(1-2):117–124.

[22] Lin JS, Zhou Y. Can scratch tests give fracture toughness? Engineering Fracture Mechanics. 2013;109:161–168.

[23] Akono AT, Ulm FJ, Bažant ZP. Discussion: Strength-to-fracture scaling in scratching. Engineering Fracture Mechanics. 2014;119:21–28.

[24] Lin JS, Zhou Y. Rebuttal: Shallow wide groove scratch tests do not give fracture toughness. Engineering Fracture Mechanics. 2015;133:211–222.

[25] Le JL, Detournay E. Discussion on the "Fracture Mechanics Interpretation of the Scratch Test" by Akono et al. Engineering Fracture Mechanics. 2016;(168):46–50.

[26] Akono AT, Bouché GA. Rebuttal: Shallow and deep scratch tests as powerful alternatives to assess the fracture properties of quasi-brittle materials. Engineering Fracture Mechanics. 2016;158:23–38.

[27] Zhou Y. Discussion on the interpretation of scratch tests with size effect law. Engineering Fracture Mechanics. 2017;100(169):178–183.

[28] Akono AT. Reply to "Discussion on the Fracture mechanics interpretation of the scratch test by Akono et al.". Engineering Fracture Mechanics. 2017;178:14–21.

[29] Wei X, Wang CY, Yuan HL, Xie Z. Study of fracture mechanism of rock cutting. In: Key Engineering Materials. vol. 250. Trans Tech Publ; 2003. p. 200–208.

[30] Liu H, Kou S, Lindqvist PA. Numerical simulation of the fracture process in cutting heterogeneous brittle material. International journal for numerical and analytical methods in geomechanics. 2002;26(13):1253–1278.

[31] Liu W, Zhu X. Experimental study of the force response and chip formation in rock cutting. Arabian Journal of Geosciences. 2019;12(15):1–12.

[32] Zeuch D, Finger J, et al. Rock breakage mechanisms with a PDC cutter. In: SPE Annual Technical Conference and Exhibition. Society of Petroleum Engineers; 1985. .

[33] Mishnaevsky L. Physical mechanisms of hard rock fragmentation under mechanical loading: a review. In: International Journal of Rock Mechanics and Mining Sciences and Geomechanics Abstracts. vol. 32. Oxford; New York: Pergamon Press, 1974-c1996.; 1995. p. 763.

[34] Verhoef P, Ockeloen J, Kesteren W. The significance of rock ductility for mechanical rock cutting. In: 2nd North American Rock Mechanics Symp; 1996. p. 709–716.

[35] Aresh B. Fundamental study into the mechanics of material removal in rock cutting. Northumbria University; 2012.

[36] Cheng Z, Sheng M, Li G, Huang Z, Shi H, Dai X, et al. Cracks imaging in linear cutting tests with a PDC cutter: Characteristics and development sequence of cracks in the rock. Journal of Petroleum Science and Engineering. 2019;179:1151–1158.

[37] Deliac EP, Fairhurst CE, et al. Theoretical and practical investigations of improved hard rock cutting systems. In: The 29th US Symposium on Rock Mechanics (USRMS). American Rock Mechanics Association; 1988. .

[38] He X, Xu C. Specific energy as an index to identify the critical failure mode transition depth in rock cutting. Rock Mechanics and Rock Engineering. 2016;49(4):1461–1478.

[39] Munoz H, Taheri A, Chanda E. Rock cutting characteristics on soft-to-hard rocks under different cutter inclinations. International Journal of Rock Mechanics and Mining Sciences. 2016;100(87):85–89.

[40] Percival DB, Walden AT. Wavelet methods for time series analysis. vol. 4. Cambridge university press; 2000.

[41] Che D, Zhang W, Zhu Z, Ehmann KF. Rock fails in shearing as a tuned critical system. International Journal of Rock Mechanics and Mining Sciences. 2018;110:133–139.

[42] Dai X, Huang Z, Shi H, Cheng Z, Xiong C, Wu X, et al. Rock failure analysis based on the cutting force in the single PDC cutter tests. Journal of Petroleum Science and Engineering. 2020;194:107339.

[43] Gray KE, Armstrong F, Gatlin C, et al. Two-dimensional study of rock breakage in drag-bit drilling at atmospheric pressure. Journal of Petroleum Technology. 1962;14(01):93–98.

[44] Guo H, Aziz N, Schmidt L. Rock cutting study using linear elastic fracture mechanics. Engineering fracture mechanics. 1992;41(5):771–778.

[45] Lindqvist PA. Energy consumption in disc cutting of hard rock. In: Tunnelling 82: Proceedings of the 3rd International Symposium. vol. 20. London: IMM; 1982. p. 189–196.

[46] Cheng Z, Sheng M, Li G, Huang Z, Wu X, Zhu Z, et al. Imaging the formation process of cuttings: Characteristics of cuttings and mechanical specific energy in single PDC cutter tests. Journal of Petroleum Science and Engineering. 2018;171:854–862.

[47] Walker D, Shaw M. A physical explanation of the empirical laws of comminution. AIME Trans. 1954;199:313–320.

[48] Teale R. The concept of specific energy in rock drilling. In: International journal of rock mechanics and mining sciences & geomechanics abstracts. vol. 2. Elsevier; 1965. p. 57–73.